electronics

MDPI

Article

Impact of Titanium Cranial Implants on the Electric Field and SAR Distribution Induced by Mobile Phones Within the User's Head

Dragana Živaljević [1,*], Dejan Jovanović [1], Dragan Krasić [2], Nenad Cvetković [1] and Bojana Petković [3]

[1] Faculty of Electronic Engineering, University of Nis, 18000 Nis, Serbia; dejan.jovanovic@elfak.ni.ac.rs (D.J.); nenad.cvetkovic@elfak.ni.ac.rs (N.C.)
[2] Faculty of Medicine, University of Nis, 18000 Nis, Serbia; dragan.krasic@medfak.ni.ac.rs
[3] Advanced Electromagnetics Group, Technische Universität Ilmenau, 98693 Ilmenau, Germany; bojana.petkovic@tu-ilmenau.de
* Correspondence: dragana.zivaljevic@elfak.ni.ac.rs; Tel.: +381-18529136

Abstract: The purpose of this study was to determine the impact of a titanium cranial implant on the electric field distribution and the amount of energy absorbed from a cell phone within the human head. Three-dimensional lifelike models of the head of the mobile phone user, a titanium cranial implant, and a smartphone model was built. The head model consisted of sixteen homogeneous, isotropic domains, with permittivity and conductivity parameters taken from the literature. Numerical calculations were performed at the mobile communication frequency of 2600 MHz for a head model with and without a titanium cranial implant, in order to determine a field perturbation introduced by the implant. Our results show that in the presence of a titanium cranial implant, the electric field amplitude and SAR (Specific Absorption Rate) are increased within the layers close to the outer surface of the model (skin, fat tissue, and muscle). On the other hand, a cranial implant leads to a lower penetration depth, decreasing the electric field amplitude and SAR inside the skull, cerebrospinal fluid, and brain.

Keywords: cranial implant; electromagnetic radiation; mobile phone; specific absorption rate

Citation: Živaljević, D.; Jovanović, D.; Krasić, D.; Cvetković, N.; Petković, B. Impact of Titanium Cranial Implants on the Electric Field and SAR Distribution Induced by Mobile Phones Within the User's Head. *Electronics* **2024**, *13*, 4551. https://doi.org/10.3390/electronics13224551

Received: 11 October 2024
Revised: 4 November 2024
Accepted: 13 November 2024
Published: 20 November 2024

1. Introduction

The treatment of bone defects in the craniofacial and maxillofacial regions is a very common clinical problem. Bone defects usually arise from musculoskeletal tumors, infections, or trauma. Diagnostics and therapy require accurate three-dimensional representation of bones and soft tissues. This representation is enabled using magnetic resonance tomography (MRT).

Along with the development of technical imaging capabilities and the improvement of surgical instruments, the materials for the reconstruction of certain bone defects have also been developed. These materials have to be biocompatible and have to meet certain criteria [1]. In this context, titanium has demonstrated excellent performance and is often used in place of many other metals. Its chemical and mechanical characteristics and possible tissue reactions are presented in [2].

Since the penetrated electromagnetic field is influenced by the composition, morphology, and size of biological organs, it is logical to assume that the presence of a metal object will affect the distribution of the electromagnetic field in its vicinity [3–6].

Studies [7–12] have previously examined the effects of various implants, such as wires, rods, orthopedic implants, pacemakers, auditory implants, and coronary stents, on the distribution of electromagnetic fields. In these studies, an analysis of RF far-field exposure was performed. Hence, it is not possible to draw any conclusions based on the findings of these studies regarding RF near-field exposure, which is the case when the source of

electromagnetic radiation is a mobile phone, positioned near to the user's head. Virtanen et al. [13] estimated the specific energy absorption rate inside a head with authentic metallic implants exposed to a half-wave dipole antenna. In [14], the influence of a head implant on the absorbed energy distribution is considered, but in the vicinity of the wireless power transfer embedded smart table.

The aim of this study is to model the titanium cranial implant and then analyze its influence on the electromagnetic field distribution and the amount of absorbed energy induced by a mobile phone within certain biological structures of the user's head.

Since it is considered unethical to perform tests on human subjects, the best evaluation of RF radiation effects is to use numerical simulations. The effects of exposure to electromagnetic radiation are usually evaluated by analyzing the penetrated electromagnetic field and SAR within the biological organs. To achieve this, 3D realistic numerical models have been created that provide reliable results regarding the penetrated electromagnetic field and the amount of absorbed energy from the mobile phone RF radiation inside the user's head. The Computer Simulation Technology (CST) [15] software (2012) package was used to perform numerical simulation of the E-field and SAR values at the frequency of 2600 MHz.

Our model includes the fourth generation of mobile communication standards available in the Republic of Serbia. The penetrated SAR and electric field values will be compared to those allowed in the territory of this country [16].

2. Models and Methods

2.1. Head Model

A three-dimensional lifelike model of a mobile phone user comprises sixteen biological tissues and organs: skin, fatty tissue, muscle, skull, mandible, tongue, eyes, teeth, vertebrae, cartilage, thyroid gland, cerebrospinal fluid, cerebrum, cerebellum, brain stem, and hypophysis. The anterior and side views of a realistic 3D head model are presented in Figures 1a and 1b, respectively. Transverse, sagittal, and coronal cross-sections are represented in Figures 2a, 2b and 2c, respectively.

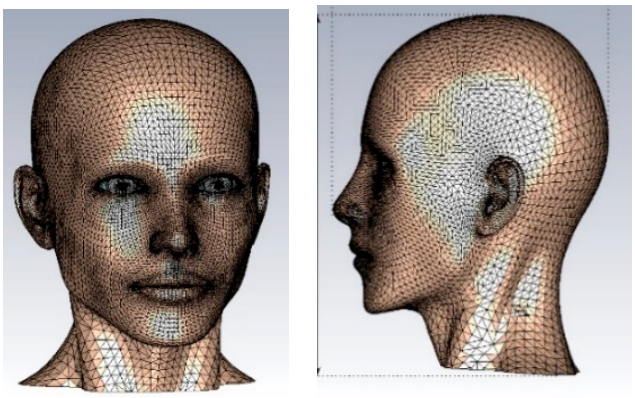

(**a**) (**b**)

Figure 1. A realistic 3D head model: anterior view (**a**) and side view (**b**).

When the 3D head model is created, it is essential to allocate suitable electromagnetic characteristics to each tissue in the head. These properties are frequency-dependent, so values for a specific frequency of 2600 MHz are needed. We use relative permittivity (ε_r), an electrical conductivity (σ), and a tissue density (ϱ) at the operating frequency of 2600 MHz as shown in Table 1 [17]. The effects of electromagnetic wave reflection, propagation, and attenuation within the user's head are greatly influenced by these characteristics of biological tissues.

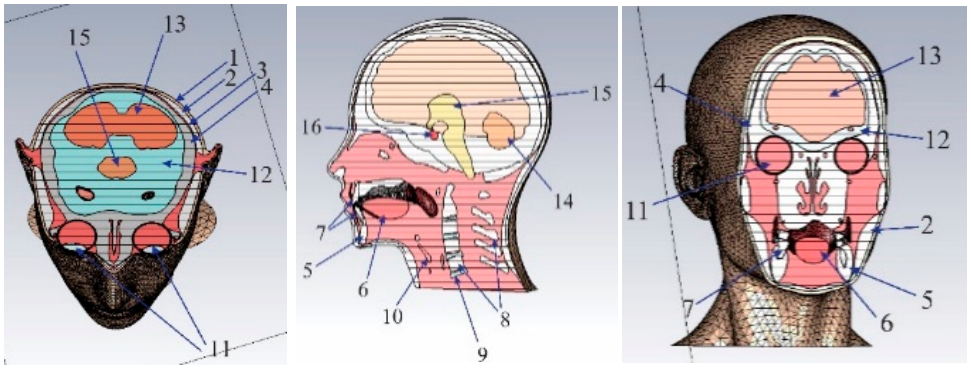

(**a**) (**b**) (**c**)

Figure 2. Cross sections of the head model: transverse (**a**), sagittal (**b**), and coronal (**c**).

Table 1. Electromagnetic properties of biological tissues and organs at 2600 MHz.

Biological Tissue		ε_r	**σ [S/m]**	**ϱ [kg/m^3]**
1.	Skin	37.8	1.54	1109
2.	Fat	10.8	0.29	911
3.	Muscle	52.5	1.84	1090
4.	Skull	14.8	0.64	1543
5.	Mandible	11.3	0.42	1908
6.	Tongue	52.4	1.92	1090
7.	Teeth	11.3	0.42	2180
8.	Vertebrae	11.3	0.42	1908
9.	Cartilage	38.4	1.87	1100
10.	Thyroid gland	57.0	2.09	1050
11.	Eyes *	47.55	2.08	1060
12.	Cerebrospinal fluid	66.0	3.60	1007
13.	Cerebrum	44.5	2.20	1046
14.	Cerebellum	44.5	2.20	1045
15.	Brain stem	44.5	2.20	1046
16.	Pituitary gland	57.0	2.09	1053

* Characteristics of tissues are defined as an average value.

The Table provides data on the dielectric characteristics of all tissues at a particular frequency. The dielectric characteristics rely on the Gabriel dispersion equations [18]. They are calculated from measurements of the impedance of a sample, performed using an automatic swept frequency network and impedance analyzers. Dispersion has been taken into consideration using complex permittivity values in numerical simulations.

2.2. Model of a Cranial Implant

A 3D model of a cranial implant is created using 3D images of real implants, installed due to existing bone tissue defects or defects resulting from certain surgical interventions. A model of a cranial implant used in our simulations is presented in Figure 3. The implant is placed on the right side of the head, i.e., the same side as the electromagnetic field radiation (mobile phone) source.

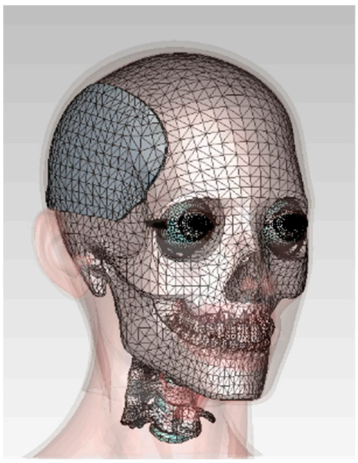

Figure 3. 3D numerical model of cranial implant.

As previously mentioned, the most frequently used material for cranial implants is titanium. Therefore, for the purposes of this numerical calculation, the electromagnetic characteristics of titanium have been used for the model of the cranial implant.

The cranial implant is a titanium alloy implant fabricated using electron beam melting [19]. It has of a volume 18.77 cm^3 and a density ϱ = 4.5 g/cm^3, producing a total mass of 84.46 g. The thickness of the implant is between 1.8 mm and 2.3 mm. The material is non-magnetic with a relative permeability of 1.00005. Its electrical resistivity is equal to 42 μΩ cm.

2.3. Model of a Smartphone

For the purpose of the current investigation, the smartphone as an electromagnetic radiation source, was modeled. A planar inverted F antenna (PIFA) serves as the electromagnetic radiation source. One way of its design and analysis with a MIMO system is proposed in [20]. The PIFA has been modeled for the frequency of 2.6 GHz with the output power of 1 W [21] and an impedance of Z = 50 Ω. The 3D model of a cellphone comprises a housing, camera, battery, display, antenna, and PCB board.

The position of a mobile phone in relation to the 3D head model is shown in Figure 4a. Figure 4b shows the PIFA inside a model of a mobile phone. The shortest distance between the surface of the head and the antenna is equal to 6 mm. S-parameters of the antenna are shown in Figure 5.

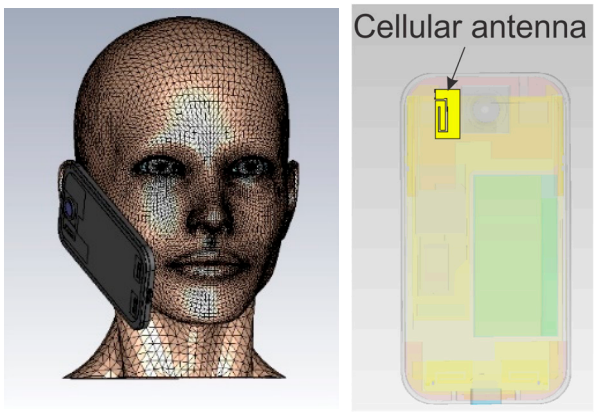

(**a**) (**b**)

Figure 4. 3D numerical model of a mobile phone and its relative position to the head (**a**); model of the planar inverted F antenna inside a phone (**b**).

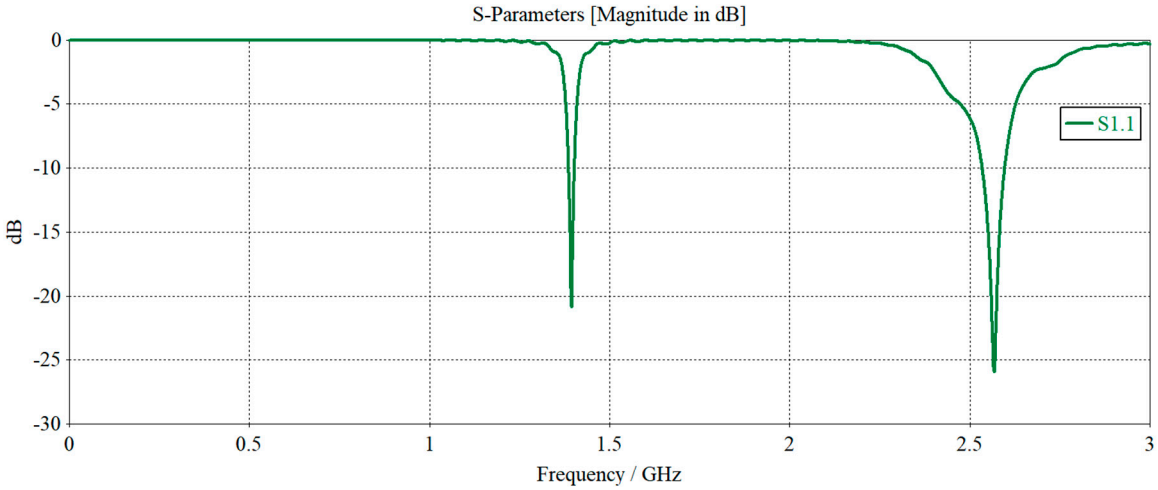

Figure 5. S-parameters of the planar inverted F antenna.

2.4. Finite Integral Technique

In order to simulate the propagation of electromagnetic waves of a mobile phone inside biological organs in the presence of a cranial implant, the CST Studio Suite [15] software (Version 12) package based on the Finite Integral Technique (FIT) [22] was used. This software for solving 3D electromagnetic problems offers an excellent CAD interface for designing and editing models while importing and exporting tools enable the utilization of models created with various 3D modeling software.

Each biological tissue and organ that is an integral part of the head modelwas modeled separately using an appropriate software package for 3D modeling. Once created, the elements of the modeled biological tissue and organs are imported into CST and linked into a unique entity with other elements. The accurate position of each tissue is defined by CT scans of the human head. Additionally, accurate modeling of separating surfaces between neighboring tissues with no overlapping is of crucial importance. This enables the application of proper boundary conditions at the surfaces separating different biological compartments. Derivation of boundary conditions is based on an integral form of Maxwell's equations and grid Maxwell's equations, using the approach introduced in [23].

Our model comprises 46,801,112 hexahedral elements. The simulations were performed with an Intel(R) Core(TM) i7-8700 K CPU @ 3.70 GHz processor, with 32 GB RAM memory within 7 h. Calculation of SAR, which belongs to the postprocessing step, requires an additional sixty minutes.

3. Results

3.1. Electric Field Distribution Within the User's Head Model

First, we investigated the distribution of the electric field in the transverse cross-section presented in Figure 6, for the case with and without a cranial implant. The position of the plane corresponds to the position of the mobile phone antenna, i.e., the position of the titanium cranial implant. A calculation line C at the transversal plane and perpendicular to the mobile phone is presented in Figure 6 as well.

The distribution of the electric field strength at the transversal cross-section (Figure 6) is presented for the case of the model containing a cranial implant and without a cranial implant in Figures 7a and 7b, respectively. The same color legend applies to both cases in order to enable a fast comparative analysis.

According to the electric field distributions within both user's head models (with and without cranial implant), represented in Figure 7, a noticeable variation in the strength of the electric field exists among specific biological tissues and organs.

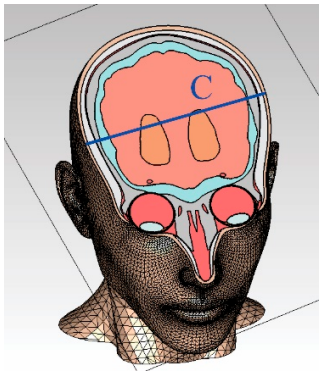

Figure 6. Calculation line C at the transversal plane, perpendicular to the mobile phone, utilized to analyze the results.

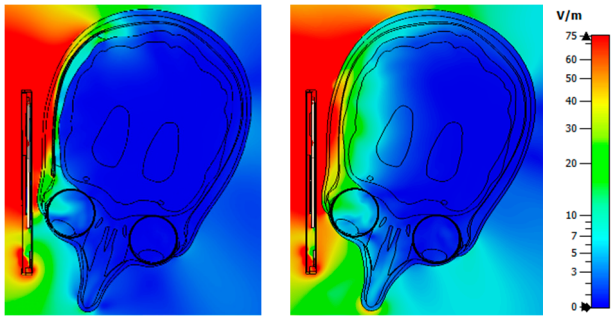

(**a**) (**b**)

Figure 7. Electric field distribution within the user's head model: (**a**) with cranial implant and (**b**) without cranial implant.

To conduct more precise assessments of the results, the dependence of electric field strength on the distance from the radiation source, along line C (shown in Figure 6), is illustrated in Figure 8, for both models.

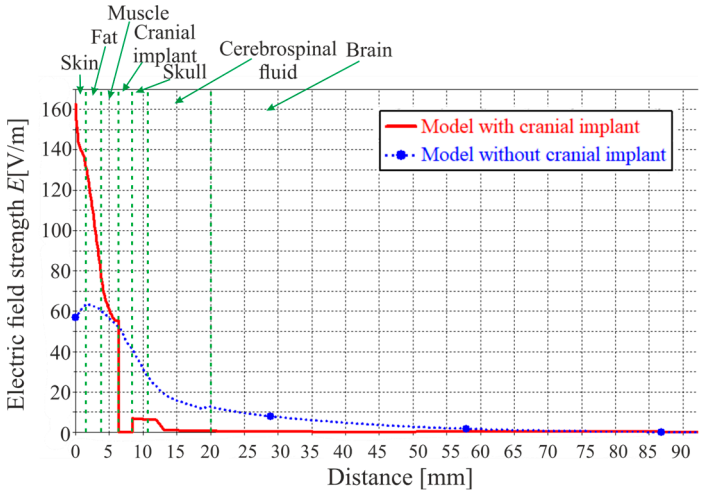

Figure 8. Electric field strength along curve C.

Comparing the numerical calculation results shown in Figure 8, for the model with and without a cranial implant, it is evident that the presence of the cranial implant leads to a notable difference in the electric field distribution.

3.2. SAR Distribution Within the User's Head Model

The basic limit for the exposure of the population to electromagnetic fields refers to exposure to variable electromagnetic fields, low-frequency or high-frequency. Basic limits and reference levels for exposure to electromagnetic radiation are generally based on established health and biological effects. One of the physical quantities used to model these limitations is the specific level of energy absorption, or SAR (Specific Absorption Rate).

SAR is a measure of the interaction between an electromagnetic wave and biological tissue, i.e., a measure of the rate at which the human body absorbs energy per unit mass of biological tissue exposed to electromagnetic radiation. SAR can be determined by the following equation [24]:

$$SAR = \frac{\sigma}{\rho}|E|^2, \tag{1}$$

where σ is the electrical conductivity (S/m), and ρ is the density of the tissue or biological organ (kg/m^3). E represents the root mean square (rms) value of the electric field.

SAR is commonly described for either the entire body or specific body regions and is measured in watts per kilogram. Equally important and suitable for application in practice is the average SAR. In addition to SAR being averaged over the volume of the whole body, local averaged SAR values are often necessary to reduce the overexposure to electromagnetic radiation on specific smaller body parts. One example of this scenario is when a person is exposed to electromagnetic radiation from a mobile phone antenna.

The average SAR is determined by integrating the local SAR expression with the desired volume of the biological tissue and dividing it by the corresponding volume:

$$SAR_{\mathrm{AV}} = \frac{1}{V}\int_V SAR\,\mathrm{d}V = \frac{1}{V}\int_V \frac{\sigma E^2}{\rho_m}\,\mathrm{d}V. \tag{2}$$

The local SAR is calculated by averaging over a small sample volume. The sample is usually 1 g or 10 g of tissue, defining a local SAR_{1g} and a local SAR_{10g}, respectively. Since spatial averaging is performed over different size regions for both measures, the differences in local SAR distributions occur. The averaging procedure can also affect the location of the highest SAR value. Therefore, both measures, the local SAR_{1g} and local SAR_{10g}, are used for predicting the energy absorbed per unit mass when exposed to an electromagnetic field. SAR averaging in this study was performed according to the international standard [25].

The distributions of SAR_{1g} and SAR_{10g} for both models (with and without a cranial implant), for the cross-section represented in Figure 6, are shown in Figures 9 and 10, respectively. In order to make a better comparison of the results obtained, the highest SAR value in the color palette is identical for both models.

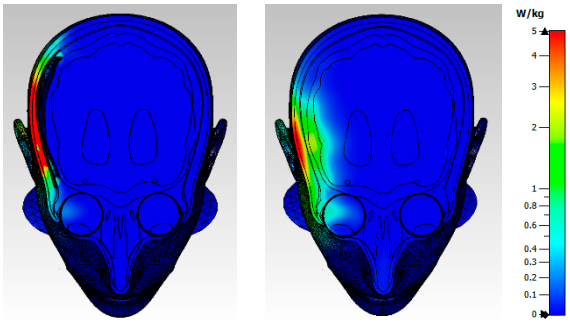

(**a**) (**b**)

Figure 9. Spatial distribution of SAR_{1g} inside the user's head model: (**a**) with cranial implant and (**b**) without cranial implant.

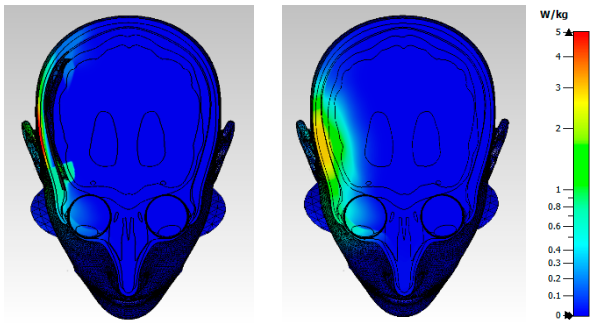

Figure 10. Spatial distribution of SAR_{10g} inside the user's head model: (**a**) with cranial implant and (**b**) without cranial implant.

In order to evaluate the impact of the titanium cranial implant on the SAR distribution inside the user's head model, the graphs of SAR_{1g} and SAR_{10g} values vs. radiation source distance (Figure 5), along line C, are shown in Figures 11 and 12, respectively.

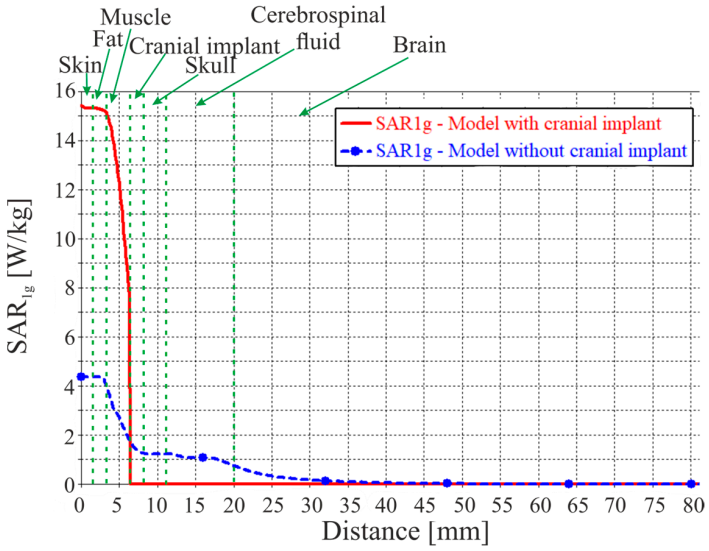

Figure 11. Specific absorption rate—SAR_{1g} along line C.

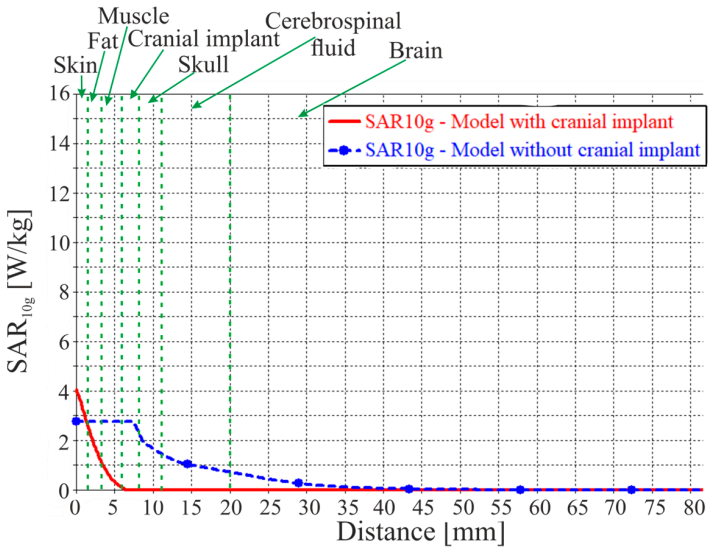

Figure 12. Specific absorption rate—SAR_{10g} along line C.

According to the graphs presented in Figures 11 and 12, it can be noticed that the distribution of SAR_{1g} as well as SAR_{10g} is different for both models (model with and model without a cranial implant) within certain biological structures. Also, by analyzing the obtained results shown in Figures 11 and 12, significant differences in the highest SAR_{1g} and SAR_{10g} values within individual biological tissues can be observed.

4. Discussion

Results shown in Figure 7 indicate that the strength of the electric field is higher in the layers close to the outer boundary of the head (skin, fatty tissue, and muscle) of the model that includes the titanium cranial implant. However, it is noticeable that the obtained distribution of the electric field within the skull, cerebrospinal fluid, and brain indicates a higher intensity of the electric field in these tissues for the model without the titanium cranial implant.

Similar conclusions can be drawn from the results presented in Figure 8. The greatest increase in electric field intensity occurs within the model with a titanium cranial implant, especially in the superficial biological tissue. Examining the differences in electric field intensity between the model with a cranial implant and the one without, it is evident that the presence of cranial implants affects the electric field distribution across the skin, adipose tissue, and muscle.

Through the analysis of the results obtained for the electric field strength along line C, it can be seen that the maximum difference in electric field intensity within the skin is 105.62 V/m. In the scenario where the model includes a cranial implant, the highest electric field value within the skin reaches 162.55 V/m, whereas for the model without the cranial implant, this value is 56.93 V/m.

There is a 71.13 V/m difference in the electric field strength within the fat tissue i.e., the highest electric field strength is 134.43 V/m with a cranial implant and 63.30 V/m without. The electric field strength inside the muscle tissue has a smaller difference in value, measuring at 24.13 V/m. In the model with the cranial implant, the highest electric field inside the muscle reaches 84.85 V/m, compared to 60.72 V/m in the model without the implant.

However, for other biological tissues and organs (skull, cerebrospinal fluid, and brain), the obtained values of the electric field strength are higher for the model without the cranial implant. The value of the electric field inside the skull in the case of the model without a cranial implant is higher by 34.58 V/m compared to the model with a cranial implant. This difference in the value of the electric field strength within the cerebrospinal fluid is 20.21 V/m, while inside the brain it is lower and amounts to 12.04 V/m.

From Figure 8, it can be also seen that the electric field intensity for the model without the cranial implant drops to a value close to zero after a penetration depth of about 70 mm. The depth of the electric field penetration is significantly smaller in the model with a cranial implant and is close to 25 mm, which results in electric field values inside the brain of less than 1 V/m.

When it comes to the amount of energy absorbed by the user's head tissues, it is evident from Figures 11 and 12 that the presence of the titanium plate affects the spatial distribution of SAR_{1g} as well as SAR_{10g}.

As in the case of electric field intensity, the largest deviation of SAR_{1g} is noticeable inside the skin, where the maximum value of SAR_{1g} for the model with a cranial implant is 11.05 W/kg higher, compared to the value obtained for the model without this implant. The maximum value of SAR_{1g} inside the skin, for the model with the cranial implant, is 15.42 W/kg, while this value is 4.37 W/kg for the model without the implant. A slightly smaller difference for the maximum value of SAR_{1g} was obtained within fatty tissue and amounts to 10.89 W/kg. A similar difference can be observed also within muscle tissue and amounts to 10.83 W/kg. According to the graph shown in Figure 11, it can be noticed that the value of SAR_{1g} inside the tissues behind the cranial implant (skull, cerebrospinal

fluid, and brain) falls to a value of 0 W/kg, while those values for the model without the cranial implant are 1.73 W/kg, 1.24 W/kg, and 0.78 W/kg, respectively.

Based on the results obtained for SAR_{10g} along curve C (Figure 12), it can be concluded that SAR_{10g} is higher only within the skin for the model with a cranial implant. The maximum value of SAR_{10g} inside the skin for the model with a cranial implant is 4.08 W/kg, while this value is 2.81 W/kg without the implant. Within the other biological tissues, it can be concluded from Figure 12 that the maximum values of SAR_{10g} are higher in the model without the cranial implant. As in the case of SAR_{1g}, the value of SAR_{10g} drops to 0 W/kg within the biological tissues located behind the cranial implant in relation to the source of electromagnetic radiation.

The local SAR_{10g} values (Figure 12) are smaller than the local SAR_{1g} values (Figure 11) at the same points of the head model. This difference in local SAR distributions occurs because spatial averaging is performed over different size regions. The increased averaging volumes in SAR_{10g} calculations result in a larger spatial smoothing effect. The SAR_{10g} typically underestimates the locally absorbed electromagnetic energy, especially in regions with relatively focused SAR local maxima.

According to standard [16], the maximal calculated SAR_{1g}, SAR_{10g}, and electric field values for the head without an implant occur inside the skin and exceed the limits 2.2, 1.4, and 2.3 times, respectively. These values for the head with an implant are 7.7, 2.04, and 6.7, respectively. The area of the brain remains inside the safe ranges in both cases.

5. Conclusions

The presence of a titanium cranial implant inside the head of a mobile phone user increases the highest values of electric field and specific absorption rate within the surface layers of the head model (skin, fatty tissue, and muscle). This is directly caused by a reflection of the electromagnetic field induced by a mobile phone. On the other side, titanium cranial implants reduce the penetration depth of the electromagnetic wave of the radiation source, which results in lower SAR values and electric field intensity within the deeper layers of the user's head model (skull, cerebrospinal fluid, and brain). In this case, a cranial implant acts as a shield in terms of a penetrating electromagnetic field for the deeper layers of the head model (skull, cerebrospinal fluid, and brain).

SAR and electric field values in superficial head layers exceed the limits set by the standards of the Republic of Serbia [16]. The inner layers of the head remain within permissible ranges.

Our future work will focus on frequencies of the 5G generation of mobile communication networks. It will also include different orientations, locations, and sizes of implants.

Author Contributions: Conceptualization, D.Ž., D.J., D.K., N.C. and B.P.; Methodology, D.Ž., D.J. and B.P.; Software, D.J.; Validation, D.K.; Formal analysis, D.Ž.; Investigation, D.J. and N.C.; Resources, D.K.; Writing—original draft, D.Ž. and D.J.; Writing—review & editing, D.Ž. and B.P. All authors have read and agreed to the published version of the manuscript.

Funding: This research received no external funding.

Data Availability Statement: Data are contained within the article.

Conflicts of Interest: The authors declare no conflict of interest.

References

1. Potter, J.K.; Ellis, E. Biomaterials for reconstruction of the internal orbit. *J. Oral. Maxillofac. Surg.* **2004**, *62*, 1280–1297. [CrossRef] [PubMed]
2. Neumann, A.; Kevenhoerster, K. Biomaterials for craniofacial reconstruction. *GMS Curr. Top. Otorhinolaryngol. Head Neck Surg.* **2009**, *8*, Doc08. [CrossRef] [PubMed]
3. Jovanovic, B.D.; Krasic, D.J.D.; Stankovic, B.V.; Cvetkovic, N.N.; Vuckovic, D.D. Electric field and SAR distribution in the vicinity of orthodontic brace exposed to the cell phone radiation. *ACES J.* **2019**, *34*, 1904–1914.

4. Whittow, W.G.; Edwards, R.M.; Panagamuwa, C.J.; Vardaxoglou, J.C. Effect of tongue jewellery and orthodontist metallic braces on the SAR due to mobile phones in different anatomical human head models including children. In Proceedings of the Loughborough Antennas and Propagation Conference, Loughborough, UK, 17–18 March 2008. [CrossRef]
5. Mortazavi, S.M.J.; Paknahad, M.; Khaleghi, I.; Eghlidospour, M. Effect of radiofrequency electromagnetic fields (RF-EMFS) from mobile phones on nickel release from orthodontic brackets: An in vitro study. *Int. Orthod.* **2018**, *16*, 562–570. [CrossRef] [PubMed]
6. Fujii, Y. Gold alloy dental inlay for preventing involuntary body movements caused by electromagnetic waves emitted by a cell phone. *IEEE Open J. Antennas Propag.* **2014**, *2*, 37–43. [CrossRef]
7. Chou, C.K.; McDougall, J.A.; Chan, K.W. RF heating of implanted spinal fusion stimulator during magnetic resonance imaging. *IEEE Trans. Biomed. Eng.* **1997**, *44*, 367–373. [CrossRef] [PubMed]
8. Hocking, B.; Joyner, K.H.; Fleming, A.H. Implanted medical devices in workers exposed to radio-frequency radiation. *Scand. J. Work Environ. Health* **1991**, *17*, 1–6. [CrossRef] [PubMed]
9. Fleming, A.H.J.; Anderson, V.; Rowley, J.R. Computational estimate of the frequency response of metallic implants in biological tissues exposed to RF fields. In Proceedings of the ACES Annual Review of Progress in Applied Computational Electromagnetics, Monterey, CA, USA, 16–20 March 1999.
10. Cooper, J.; Hombach, V. Increase in specific absorption rate in human heads arising from implantations. *Electron. Lett.* **1996**, *32*, 2217–2219. [CrossRef]
11. Foster, K.R.; Goldberg, R.; Bonsignore, C. Heating of cardiovascular stents in intense radio frequency magnetic fields. *Bioelectromagnetics* **1999**, *20*, 112–116. [CrossRef]
12. Crouzier, D.; Selek, L.; Martz, B.-A.; Dabouis, V.; Arnaud, R.; Debouzy, J.-C. Risk assessment of electromagnetic fields exposure with metallic orthopedic implants: A cadaveric study. *Orthop. Traumatol. Surg. Res.* **2012**, *98*, 90–96. [CrossRef] [PubMed]
13. Virtanen, H.; Keshvari, J.; Lappalainen, R. The effect of authentic metallic implants on the SAR distribution of the head exposed to 900, 1800 and 2450 MHz dipole near field. *Phys. Med. Biol.* **2007**, *52*, 1221–1236. [CrossRef] [PubMed]
14. Shah, I.A.; Basir, A.; Cho, Y.; Yoo, H. Safety Analysis of Medical Implants in the Human Head Exposed to a Wireless Power Transfer System. *IEEE Trans. Electromagn. Compat.* **2022**, *64*, 640–649. [CrossRef]
15. *CST Microwave Studio, version 2012*; Computer Simulation Technology: Framingham, MA, USA, 2012.
16. Available online: http://demo.paragraf.rs/demo/combined/Old/t/t2009_12/t12_0270.htm (accessed on 5 September 2020).
17. IT'IS Database for Thermal and Electromagnetic Parameters of Biological Tissues. Available online: https://itis.swiss/virtual-population/tissue-properties/traceability/doi-v4-0/ (accessed on 22 February 2022).
18. Gabriel, C. *Compilation of the Dielectric Properties of Body Tissues at RF and Microwave Frequencies*; Defense Technical Information Center: Fort Belvoir, VA, USA, 1996.
19. Moiduddin, K.; Mian, S.H.; Umer, U.; Alkhalefah, H. Fabrication and Analysis of a Ti6Al4V Implant for Cranial Restoration. *Appl. Sci.* **2019**, *9*, 2513. [CrossRef]
20. Toro, J.; Choukiker, Y.K. Design and analysis of meanderline PIFA antenna with MIMO system for mobile handheld device. In Proceedings of the 2017 International Conference on Trends in Electronics and Informatics (ICEI), Tirunelveli, India, 11–12 May 2017; pp. 1061–1065.
21. IEEE Recommended Practice for Measurements and Computations of Radio Frequency Electromagnetic Fields with Respect to Human Exposure to Such Fields, 100kHz–300GHz. Available online: https://ieeexplore.ieee.org/document/1167131 (accessed on 12 November 2024).
22. Clemens, M.; Weiland, T. Discrete electromagnetism with the finite integration technique. *Prog. Electromagn. Res.* **2001**, *32*, 65–87. [CrossRef]
23. Yee, K.S. Numerical solution of initial boundary value problems involving Maxwell's equations in isotropic media. *IEEE Trans. Antennas Propag.* **1966**, *14*, 302–307. [CrossRef]
24. Ebrahimi-Ganjeh, M.A.; Attari, A.R. Interaction of dual band helical and PIFA handset antennas with human head and hand. *Prog. Electromagn. Res.* **2007**, *77*, 225–242. [CrossRef]
25. *IEC/IEEE 62704-1*; IEC/IEEE International Standard—Determining the Peak Spatial-Average Specific Absorption Rate (SAR) in the Human Body from Wireless Communications Devices, 30 MHz to 6 GHz—Part 1: General Requirements for Using the Finite-Difference Time-Domain (FDTD) Method for SAR Calculations. 27 October 2017. IEEE Standards Association: Piscataway, NJ, USA, 2017; pp. 1–86. [CrossRef]